SECED 2023 Conference
Earthquake Engineering & Dynamics for a Sustainable Future
14-15 September 2023, Cambridge, UK

ANALYSIS OF SHEAR-CRITICAL REINFORCED CONCRETE FRAMES USING THE FORCE-BASED FIBER FRAME ELEMENT

Kushan WIJESUNDARA[1] Sameera HIPPOLA[1], Yasas LAMAWANSA[1], J. CELS[2], J. THAMBOO[3], T. ROSSETTO[2]

***Abstract**: In nonlinear analysis of reinforced concrete (RC) frame structures subjected to either seismic or tsunami loadings, an accurate prediction of shear-critical element responses is vital to accurately obtain failure and the overall strength characteristics. However, existing displacement-based finite element modelling techniques require discretization of the elements in a frame structure; or compromise on accuracy by either greatly simplifying or neglecting the axial-moment-shear interaction. Therefore, this paper presents a novel force-based fiber beam-column element that can capture the complex moment-axial-shear interaction response of RC frames. This formulation includes two nested iterations at the structure and the sectional levels. The importance of the sectional level iterations is to explicitly satisfy sectional equilibrium, which is not achieved in either existing displacement or force-based line element formulations. As a result, a stable convergence of all average strain, local crack strain, and slip strain components of the constitutive relationship is ensured. The novel element is validated with experimental results of 170 tests found in the literature. It is shown that the novel element predicts the load carrying capacity well with an average experimental-to-predicted load carrying capacity ratio of 0.99 and a coefficient of variation of 12.8%. Furthermore, the element can be used to simulate different failure mechanisms of reinforced concrete frame elements.*

KEYWORDS: Axial-moment-shear interaction, force-based finite element formulation, nonlinear response, shear-critical reinforced concrete frames

1. Introduction

Accounting for bending moment - axial force -shear force (M-N-V) interaction in the analysis of reinforced concrete (RC) structures continues to be a challenging task. Over the years, fiber element formulations have gained popularity in modelling RC frames due to their ability to predict accurately with a low computational effort. Such fiber-based frame elements include displacement-based formulations as proposed by Ceresa et al. (2007), Navarro-Gregori et al. (2013), Li et al. (2016), and Feng et al. (2017), force-based formulations as proposed by Menegotto et al. (1973), Kaba et al. (1984), Zeris et al. (1991), Ciampi and Carlesimo (1986), Remino (2004), Mohr et al. (2010), Du et al. (2019) Sae-Long et al. (2020) and Kalliontzis and Shing (2021) or mixed finite element formulations as proposed by Taylor et al. (2003), Saritas (2009), and Saritas et al. (2009). Among these methods, element discretisation is not needed in force-based formulations as the force interpolation functions are exactly known.

A displacement-based fiber element was developed by Guner and Vecchio (2010) which can predict the M-N-V interaction of RC frames. The Disturbed Stress Field Model (DSFM) proposed by Vecchio (2000) was incorporated at the fiber level. In this formulation, a single iterative procedure based on the secant stiffness is used for the global analysis. The section level equilibrium is not directly evaluated and hence, the iterative procedure may fail to converge as the section unbalanced forces cannot be minimised within the maximum number of iterations as discussed in Guner (2008). Addressing this issue, a force-based fiber element formulation was developed by Rajapakse et al. (2019). This formulation incorporates iterative procedures both at the structure level and the section level. The structural unbalanced force is minimised through the structure level iteration, while an updated section stiffness is computed for a given section force increment during the section level iteration. The initial stiffness matrices are used for both the iterative procedures and hence requires a significant computational time.

[1] Department of Civil Engineering, University of Peradeniya, Peradeniya, Sri Lanka, kushanw@eng.pdn.ac.lk
[2] EPICentre, University College London, London, UK
[3] Department of Civil Engineering, South Eastern University of Sri Lanka, Sri Lanka

Also, the Modified Compression Field Theory (MCFT) is incorporated at the fiber level consists of a cumbersome crack check.

The proposed novel formulation aims to improve the formulation developed by Rajapakse et al. (2019) by addressing its' drawbacks. Tangent stiffness is utilized at both iteration levels in the improved formulation. The incorporation of the DSFM at the fiber level omits the requirement of the cumbersome crack check as the slip deformations are computed explicitly in the DSFM. Furthermore, the computational time is significantly reduced by assuming a parabolic shear strain profile across the depth of a section. The improved element formulation was validated against 170 RC specimens available in literature. The capability of the proposed formulation to predict the load-deformation response, load capacity and the failure mode is discussed.

2. Proposed Formulation

The displacement-controlled method of analysis is utilized in the proposed formulation which consists of four hierarchical levels namely, structure level, element level, section level and the fiber level. When a displacement increment $\{\Delta U_2\}$ is applied at the displacement controlling degrees of freedoms (DOFs), the nodal force increment $\{\Delta F\}$, and the nodal displacement increment $\{\Delta U\}$ of the structure are computed during the iterative procedure at the structure level. Furthermore, at each structure level iteration *i,* the structure stiffness matrix from the previous iteration $[K]_{i-1}$ was used to solve the incremental equilibrium equation for the load factor increment ($\Delta\lambda_i$) and the unknown displacement increment vector $\{\Delta U_1\}_i$. This iterative procedure was performed until the unbalanced force satisfies the predefined tolerance criteria at the structure level. The overview of structure determination process is shown in Figure 1. During each structure level iteration, for a known element nodal displacement increment, the incremental element nodal resisting forces are computed through the element state determination. The overview of the element state determination is shown in Figure 2. Furthermore, for a given section force increment $\{\Delta S\}_i$, the updated section deformations and the stiffness matrix are obtained through the section state determination. Figure 3 shows the overview of the section state determination.

During the j[th] iteration at the section level, the section deformation increment Δe_j, section stiffness matrix $[K^{sec}]_j$, section resisting force S_{res_j} and the section unbalanced force ΔS_{unb_j} are computed. The iterative process at the section level is carried out until the section unbalanced force satisfies the predefined tolerance. More details can be found in Hippola et al. (2019) and Hippola et al. (2021). Figure 4 presents a schematic diagram of the section state determination.

The axial stresses (σ_x), shear stresses (τ_{xy}) and stiffness of all fibers of a section need to be determined to compute S_{res_j} and S_{res_j} for a given section deformation e_j . If the strain state at a material point is known, the DSFM can be used for the computations. The strain state at a material point consists of the axial strain (ε_x), shear strain (γ_{xy}) and the transverse strain (ε_y). For a given e_j, the axial strain of a material point is obtained based on the assumption that plane sections remain in-plane, while the shear strain of a material point is obtained based on the assumption of a parabolic shear strain profile through the depth of the section. Since the transverse strain is unknown, the strain value of the previous iteration is used in the solution algorithm which is carried out to compute the transverse strain value satisfying the condition of zero transverse stress σ_y. The assumption of zero transverse stress is reasonable for sections in B-regions. This solution algorithm is also included in Figure 3. The next section includes the discussion of the constitutive model utilized to compute the stress state $\{\sigma_x \sigma_y \Gamma_{xy}\}$ when the strain state $\{\varepsilon_x \varepsilon_y \gamma_{xy}\}$ of a fiber is known.

3. Constitutive Model

The DSFM was implemented at each material point to compute its' response. It is a smeared cracked model which captures the averaged behaviour using uniaxial material models defined in principal directions. The slip deformations computed considering local equilibrium at the crack locations are also incorporated.

The total strain state $\{\varepsilon_x \varepsilon_y \gamma_{xy}\}^T$, net principal strains $(\varepsilon_{c1}, \varepsilon_{c2})$ and the principal stress orientation θ are obtained based on the known net strain state $\{\varepsilon_{tx} \varepsilon_{ty} \gamma_{txy}\}^T$ and previous slip deformations $\{\varepsilon^s_{previous}\}$ as given in Equations (1) – (3).

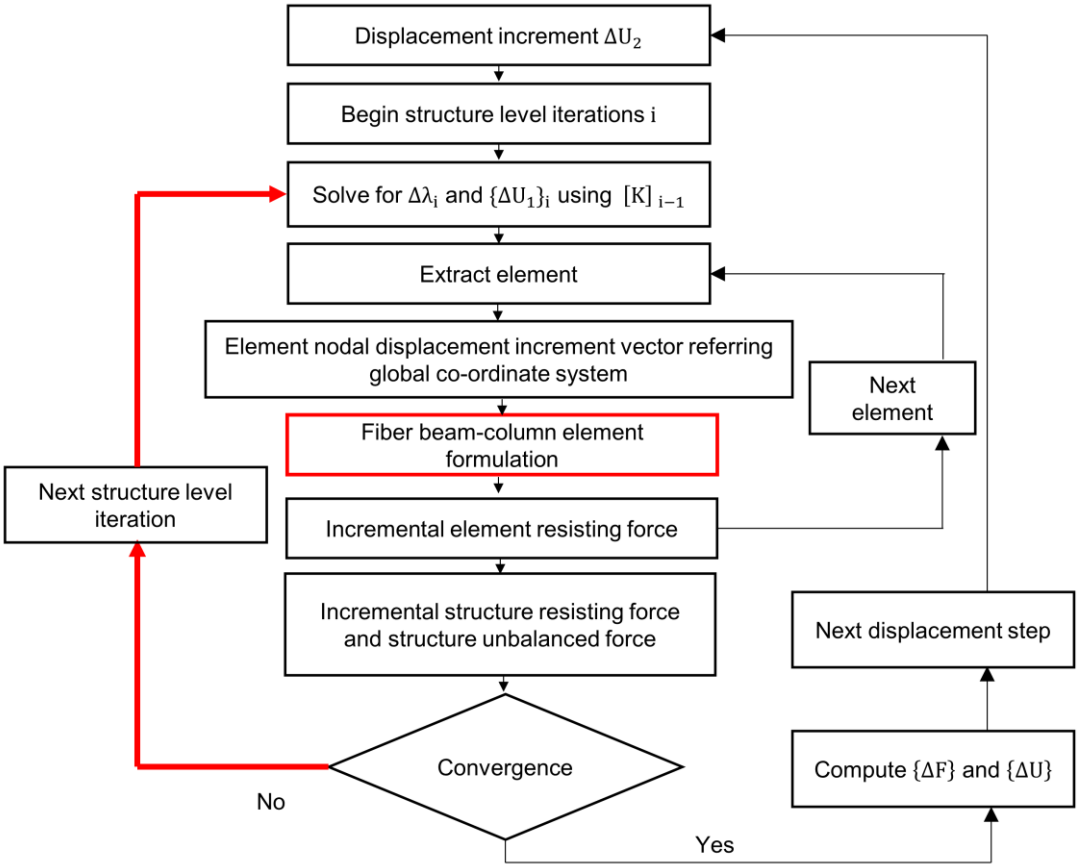

Figure 1. Structure State Determination (Hippola et al. (2022))

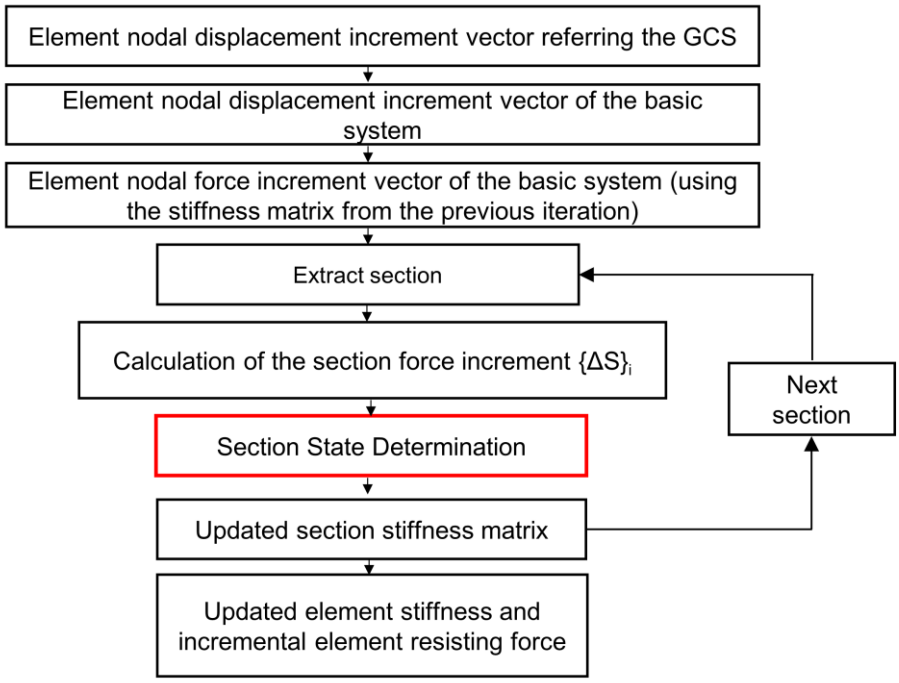

Figure 2. Element State Determination (Hippola et al. (2022))

$$\{\epsilon_{tx}\ \epsilon_{ty}\ \gamma_{txy}\}^T = \{\epsilon_x\ \epsilon_y\ \gamma_{xy}\}^T + \left\{\epsilon^s_{prev}\right\} \tag{1}$$

$$\epsilon_{c1},\epsilon_{c2} = \frac{\epsilon_x+\epsilon_y}{2} \pm \sqrt{\left(\frac{\epsilon_x-\epsilon_y}{2}\right)^2 + \left(\frac{\gamma_{xy}}{2}\right)^2} \tag{2}$$

$$\theta = \frac{1}{2}\tan^{-1}\left(\frac{\gamma_{xy}}{\epsilon_y-\epsilon_x}\right) \tag{3}$$

Then, the uniaxial constitutive relationships are used to obtain the net principal stresses (f_{c1}, f_{c2}) in concrete. The dominant mechanism out of tension stiffening as proposed by Bentz (2000) and tension softening (linear) is considered in the computations of the post-cracking principal tensile stress. Furthermore, the Modified Kent and Park model found in Kent and Park (1991) was used for the computations of the principal compressive stress. Compression softening and confining effects are also considered. Assuming a perfect bond between steel and concrete, the transverse steel stress (f_{sy}) was obtained based on a bilinear material model. Subsequently, the tangent $[D_{tangent}]$ and secant $[D_{secant}]$ fiber stiffness matrices are obtained as given in Equations (4) and (5). p_x, p_y and T_{rot} denote the reinforcement ratios of the fiber in the x,y directions and the transformation matrix respectively. The transformation matrix is given in Equation (6).

For each fiber, the local shear stresses at the cracks (V_{ci}) were then calculated based on the equilibrium, compatibility, and the constitutive relationship of steel. Both the stress-based approach proposed by Okamura and Maekawa (1991), and the constant lag-based approach described in Vecchio (2000) is used to compute the slip displacement of each fiber based on (V_{ci}). The maximum slip displacement obtained from the two approaches is used to find the slip deformation vector $\{\varepsilon^s\}$. More details of these computations can be found in Guner (2008), and Guner and Vecchio (2010). Then, the stress state of a fiber is computed as given in Equation (7). It should be noted that the computationally demanding crack check can be avoided through the explicit computation of the slip deformation.

$$[D_{tangent}] = T^T_{rot}\begin{bmatrix} \frac{df_{c1}}{d\epsilon_1} & 0 & 0 \\ 0 & \frac{df_{c2}}{d\epsilon_2} & 0 \\ 0 & 0 & \frac{0.5(f_{c1}-f_{c2})}{\epsilon_{c1}-\epsilon_{c2}} \end{bmatrix} T_{rot} + \begin{bmatrix} 0 & 0 & 0 \\ 0 & p_y\frac{df_{sy}}{d\epsilon_y} & 0 \\ 0 & 0 & 0 \end{bmatrix} \tag{4}$$

$$[D_{tangent}] = T^T_{rot}\begin{bmatrix} \frac{f_{c1}}{\epsilon_{c1}} & 0 & 0 \\ 0 & \frac{f_{c2}}{\epsilon_{c2}} & 0 \\ 0 & 0 & \frac{\frac{f_{c1}}{\epsilon_{c1}}\frac{f_{c2}}{\epsilon_{c2}}}{\frac{f_{c1}}{\epsilon_{c1}}+\frac{f_{c2}}{\epsilon_{c2}}} \end{bmatrix} T_{rot} + \begin{bmatrix} 0 & 0 & 0 \\ 0 & p_y\frac{f_{sy}}{\epsilon_y} & 0 \\ 0 & 0 & 0 \end{bmatrix} \tag{5}$$

$$T_{rot} = \begin{bmatrix} \cos^2\theta & \sin^2\theta & \cos\theta\sin\theta \\ \sin^2\theta & \cos^2\theta & -\cos\theta\sin\theta \\ -2\cos\theta\sin\theta & 2\cos\theta\sin\theta & \cos^2\theta-\sin^2\theta \end{bmatrix} \tag{6}$$

$$\begin{Bmatrix} \sigma_x \\ \sigma_y \\ \Gamma_{xy} \end{Bmatrix} = [D_{secant}]\left\{\epsilon_{tx}\ \epsilon_{ty}\ \gamma_{txy}\right\}^T - [D_{secant}]\left\{\epsilon^s_{previous}\right\} \tag{7}$$

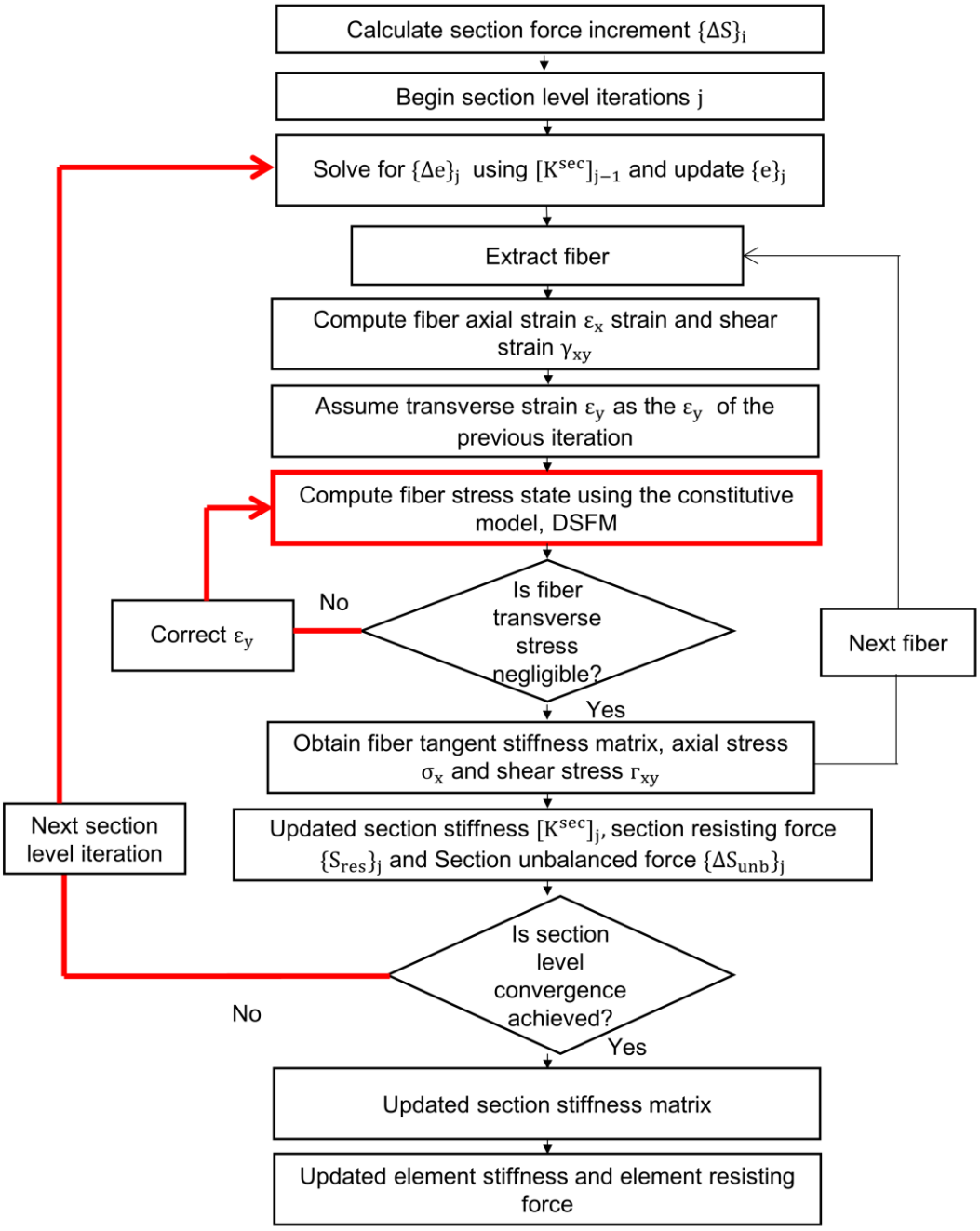

Figure 3. Section State Determination (Hippola et al. (2022))

4. Experimental Database

The specimens were selected from the experimental studies of Bresler and Scoredelis (1963). The selected specimens have varying shear span to depth ratios, longitudinal and transverse reinforcement percentages, and concrete compressive strengths The details of these specimen can be found in Hippola et al. (2022).

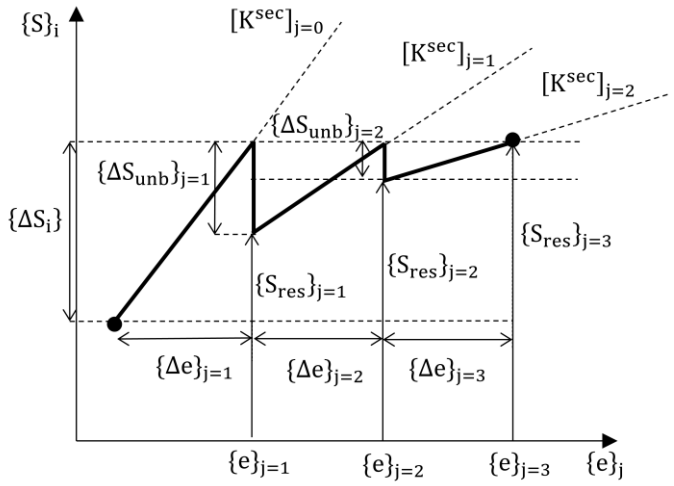

Figure 4. Schematic diagram of the iterative procedure at the section level (Hippola et al. (2022))

5. Results and Discussion

The load-deformation responses and the failure modes of selected simply supported beams obtained using the proposed formulation is discussed in this section. The beams were modelled using two elements each consisting of six integration points. Each monitoring section was discretized into sixty fiber layers. A schematic diagram of the model is given in Figure 5.

The experimental load-deformation responses of the beam test series in Bresler and Scordelis (1963) are compared with the predictions of the proposed formulation as illustrated in Figure 6. This test series is widely used to verify models for shear critical RC beams. The initial stiffness, post-cracking stiffness and load carrying capacities of the B2, C2, OA2, A3, B3, C3 and OA3 beams obtained using the proposed formulation are in good agreement with the experimental observations. An overestimation of the post-cracking stiffness was observed in the beams A1, A2, B1, C1 and OA1 which have lower shear span to depth ratios.

Three different failure modes were observed during the experiments. Namely, shear-compression failures (S-C), diagonal tension failures (D-T) and flexure-compression failures (F-C). The capability of the proposed formulation to capture the S-C and D-T failure modes is discussed herein.

5.1 Shear-compression failure

The A1 beam failed due to the crushing of concrete near the loading plate as a result of the combined action of flexure and shear. The prediction of the failure mode of the beam A1 using the proposed model is discussed here.

Variations of the principal stresses and the shear stresses across the depth at each monitoring section at the failure of the A1 beam is given in Figure 7. From Figure 7(a), it can be observed that the top fibers at the monitoring sections 5 and 6 have reached their compressive strength.

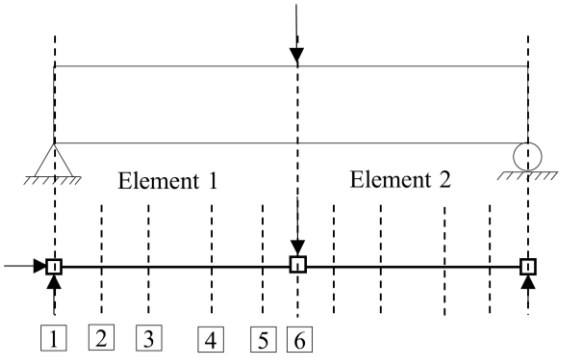

Figure 5. Schematic diagram of a beam model (Hippola et al. (2022))

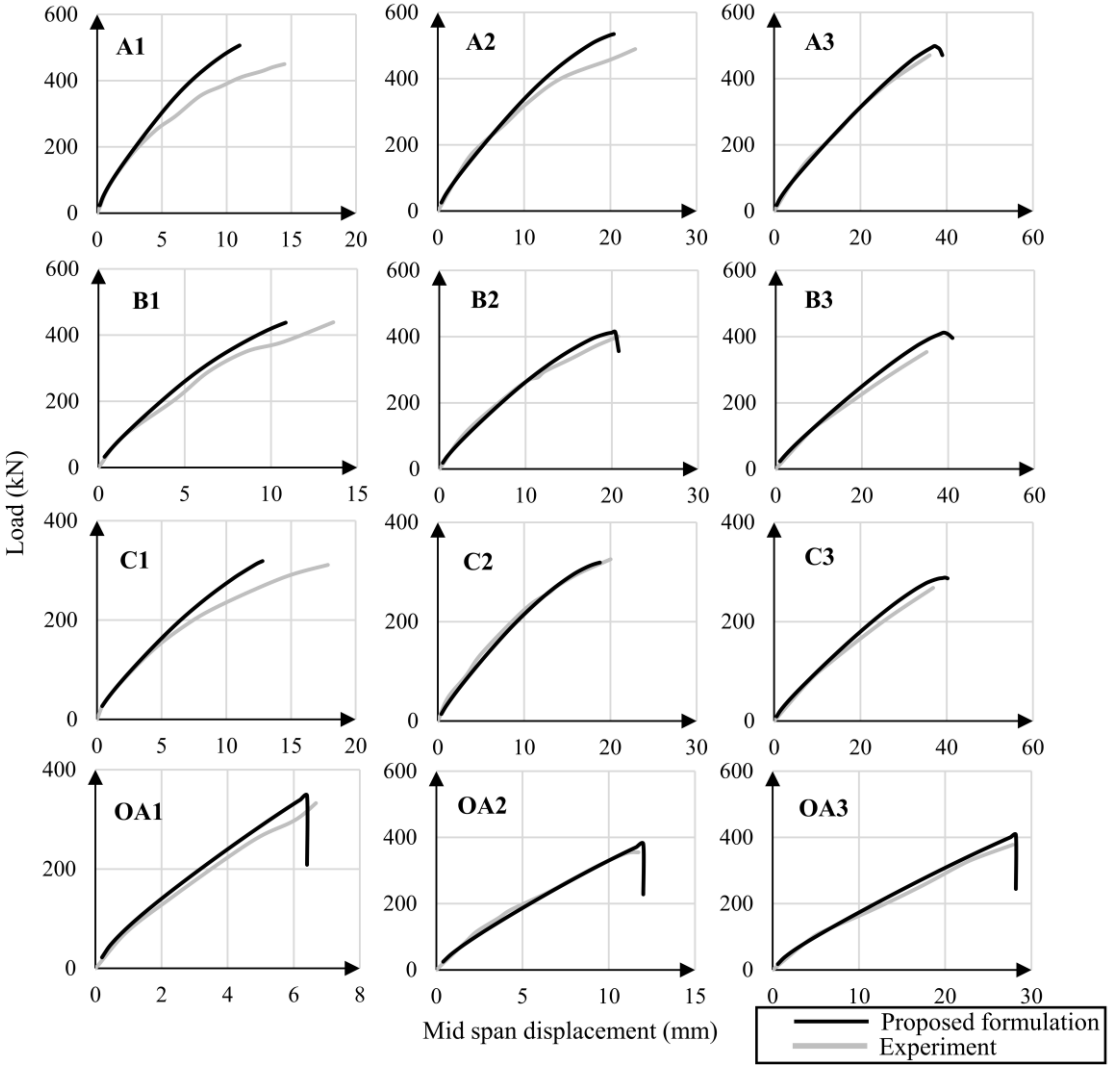

Figure 6. Load deformation responses of the Bresler and Scordelis beams (1963) (Hippola et al. (2022))

Furthermore, it is observed from Figure 7(e) that the crack orientations predicted near the loading point confirm the inclination of the principal compressive direction in concrete. Based on this observation, it can be concluded that the proposed formulation accurately predicts the crushing of concrete near the loading point is due to the combined effects of shear and bending.

5.2 Diagonal tension failure

The OA2 beam having no transverse reinforcement experimentally failed due to the formation of a single dominant D-T crack. Variations of the principal stresses and the shear stresses across the depth at each monitoring section immediately prior to the failure of the OA2 beam is given in Figure 8. In a section with no transverse reinforcement, certain fibers which are away from the longitudinal reinforcement bars will be locally unreinforced in both directions. It can be observed from Figure 8(b) that the tension softening has become zero in the fibers at the mid level of section 4 which are locally unreinforced. Hence, the prediction of cracks with large widths in such fibers infers the experimentally observed single dominant crack. It should also be noted that the shear-compression crushing which was observed near the loading in the A1 beam is not observed in this case as evident from Figure 8(a).

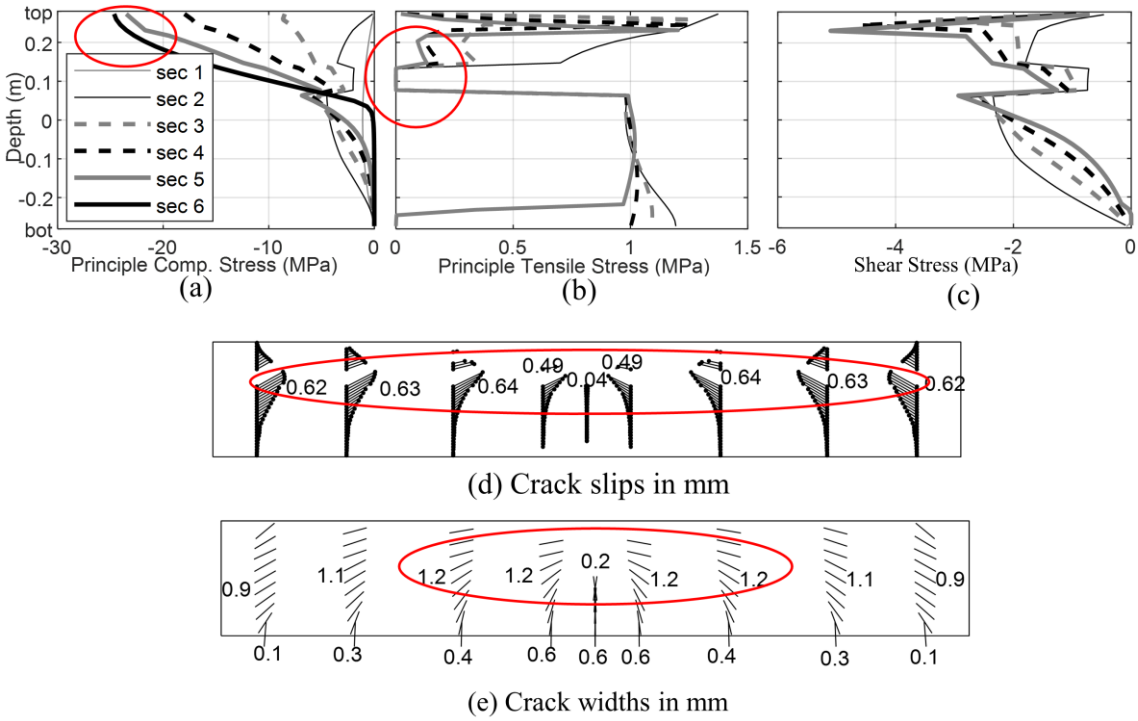

Figure 7. Plots at each monitoring section of the A1 beam at failure (Hippola et al. (2022))

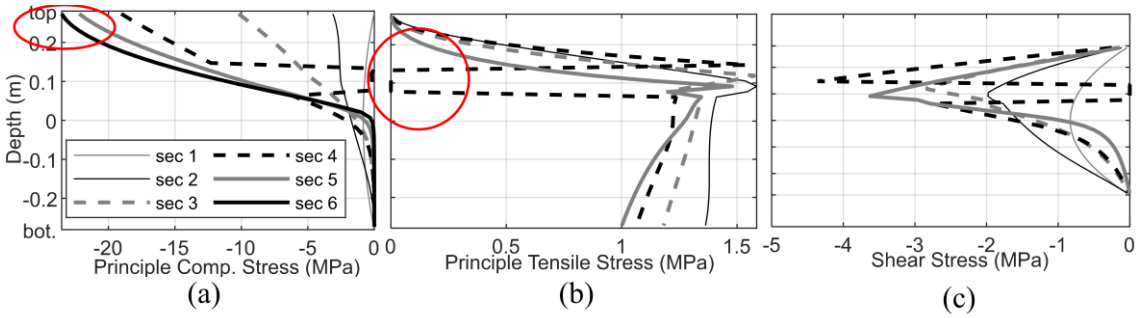

Figure 8. Plots at each monitoring section of the OA2 beam at failure (Hippola et al. (2022))

Conclusions

A novel force-based fiber element capable of capturing the N-M-V interaction of RC frame elements was developed in this study. The proposed formulation which uses the DSFM as the constitutive relationship at the fiber level consists of iterative procedures at both the structure level and the section level. Faster convergence is achieved by incorporating the respective tangent stiffness matrices during both iterative processes.

The proposed formulation was validated using experimental results of 170 specimens found in literature. The specimens include beams, walls and frames having varying shear span to depth ratios, transverse and longitudinal reinforcement percentages, and compressive strengths. Overall, the average experimental to predicted load carrying capacity ratio was 0.99 and the coefficient of variation was 12.8%.

The capability of the proposed formulation to adequately predict the load-deformation responses of RC elements was discussed in the preceding sections by comparing the load-deformation responses of the Bresler and Scordelis beams (1963) obtained using the proposed formulation with the experimental observations. Furthermore, the proposed element accurately predicted the S-C, D-T and F-C failure modes.

References

Angelakos, D., Bentz, E. C. and Collins, M. P. (2001) “Effect of concrete strength and minimum stirrups on shear strength of large members,” ACI Struct J, 98(3), pp. 290–300.

Bentz, E. C. (2000) Sectional Analysis of Reinforced Concrete Members. Toronto, ON, Canada.

Ceresa, P., Petrini, L. and Pinho, R. (2007) “Flexure-shear fiber beam-column elements for modeling frame structures under seismic loading-state of the art,” Journal of Earthquake Engineering, 11(S1), pp. 46–88.

Ciampi, V. and Carlesimo, L. A. (1986) “nonlinear beam element for seismic analysis of structures,” in Proceedings of the 8th European Conference on Earthquake Engineering. Lisbon, Portugal.

Du, Z.-L. et al. (2019) “Advanced flexibility-based beam-column element allowing for shear deformation and initial imperfection for direct analysis,” Engineering structures, 199(109586), p. 109586. doi: 10.1016/j.engstruct.2019.109586.

Duong, K. V., Sheikh, S. A. and Vecchio, F. J. (2007) “Seismic behaviour of shear-critical reinforced concrete frame: experimental investigation,” ACI Struct J, 104(3), pp. 304–313.

Feng, D.-C. et al. (2017) “A flexure-shear Timoshenko fiber beam element based on softened damage-plasticity model,” Engineering structures, 140, pp. 483–497. doi: 10.1016/j.engstruct.2017.02.066.

Guner, S. (2008) Performance Assessment of Shear-Critical Reinforced Concrete Plane Frames. Toronto, ON, Canada.

Guner, S. and Vecchio, F. J. (2010) “Pushover analysis of shear-critical frames: formulation,” ACI Struct J, 107(1), pp. 63–71.

Hippola, H. et al. (2019) “Modification of force-based fibre beam-column element formulation to cater highly localized nonlinear behaviour,” in Proceedings of the 7th ECCOMAS Thematic Conference on Computational Methods in Structural Dynamics and Earthquake Engineering. Crete, Greece.

Hippola, S. et al. (2021) “A force-based fiber beamcolumn element to predict moment-axial-shear interaction of reinforced concrete frames,” Struct Concr, 22, pp. 2466–2481.

Hippola, H.M.S.S., Wijesundara, K.K. and Nascimbene, R., 2022. Response of shear critical reinforced concrete frames and walls under monotonic loading. *Engineering Structures*, *251*, p.113483.

Kaba, S. and Mahin, S. A. (1984) Refined modeling of reinforced concrete columns for seismic analysis. Berkeley.

Kalliontzis, D. and Shing, P. B. (2021) “Force-based frame element with axial force-flexure-shear interaction for modelling reinforced concrete members,” ACI Struct J, 118(3).

Kent, D. C. and Park, R. (1971) “Flexural members with confined concrete,” Journal of the Structural Division, 97(7), pp. 1969–1990. doi: 10.1061/jsdeag.0002957.

Krefeld, W. J. and Thurston, C. W. (1966) “Studies of the shear and diagonal tension strength of simply supported reinforced concrete beams,” ACI J, 63(4), pp. 451–476.

Lefas, I. D., Kotsovos, M. D. and Ambraseys, N. N. (1990) “Behaviour of reinforced concrete structural walls: strength, deformation characteristics, and failure mechanism,” ACI Struct J, 93, pp. 23–31.

Li, Z.-X., Gao, Y. and Zhao, Q. (2016) “A 3D flexure–shear fiber element for modeling the seismic behavior of reinforced concrete columns,” Engineering structures, 117, pp. 372–383. doi: 10.1016/j.engstruct.2016.02.054.

Menegotto, M. and Pinto, P. E. (1973) “Method of analysis for cyclically loaded reinforced concrete plane frames including changes in geometry and non-elastic behaviour of elements under combined normal force and bending,” in IABSE symposium on resistance and ultimate deformability of structures acted on by well-defined repeated loads. Lisbon, Portugal.

Mohr, S., Bairán, J. M. and Marí, A. R. (2010) “A frame element model for the analysis of reinforced concrete structures under shear and bending,” Engineering structures, 32(12), pp. 3936–3954. doi: 10.1016/j.engstruct.2010.09.005.

Navarro-Gregori, J. et al. (2013) “A theoretical model for including the effect of monotonic shear loading in the analysis of reinforced concrete beams,” Engineering structures, 52, pp. 257–272. doi: 10.1016/j.engstruct.2013.02.035.

Okamura, H. and Maekawa, K. (1991) Nonlinear analysis and constitutive models of reinforced concrete. Tokyo: Giho-do Press.

Rajapakse, R. et al. (2019) “Accounting axial-moment-shear interaction for force-based fibre modeling of RC frames,” Eng Struct, 184, pp. 15–36.

Remino, M. (2004) “Shear modelling of reinforced concrete structures,” in Dipartimento di Ingegneria Civile. Brescia, Italy.

Sae-Long, W. et al. (2020) “Forced-based Shearflexure-interaction Frame Element for Nonlinear Analysis of Non-ductile Reinforced Concrete Columns,” Journal of Applied and Computational Mechanics, 6, pp. 1151–1167.

Saritas, A. (2009) “Modeling of inelastic behaviour of curved members with a mixed formulation beam element,” Finite Elem Anal Des, 45(5), pp. 357–368.

Saritas, A. and Filippou, F. C. (2009) “Inelastic axial-flexure–shear coupling in a mixed formulation beam finite element,” International journal of non-linear mechanics, 44(8), pp. 913–922. doi: 10.1016/j.ijnonlinmec.2009.06.007.

Sherwood, E., Bentz, E. and Collins, M. P. (2007) “Effect of aggregate size on beam-shear strength of thick slabs,” ACI Struct J, 104, pp. 180–190.

Taylor, R. L. et al. (2003) “A mixed finite element method for beam and frame problems,” Computational mechanics, 31(1–2), pp. 192–203. doi: 10.1007/s00466-003-0410-y.

Vecchio, F. J. (2000) “Disturbed stress field model for reinforced concrete: Formulation,” Journal of structural engineering (New York, N.Y.), 126(9), pp. 1070–1077. doi: 10.1061/(asce)0733-9445(2000)126:9(1070).

Vecchio, F. J. and Balopoulou, S. (1990) “On the nonlinear behaviour of reinforced concrete frames,” Canadian journal of civil engineering, 17(5), pp. 698–704. doi: 10.1139/l90-083.

Vecchio, F. J. and Collins, M. P. (1986) “The modified compression field theory for reinforced concrete elements subjected to shear,” ACI Journal, 83(2), pp. 219–231.

Vecchio, F. J. and Emara, M. B. (1992) “Shear deformations in reinforced concrete frames,” ACI Struct J, 89, pp. 46–56.

Vecchio, F. J. and Shim, W. (2004) “Experimental and analytical reexamination of classic concrete beam tests,” Journal of structural engineering (New York, N.Y.), 130(3), pp. 460–469. doi: 10.1061/(asce)0733-9445(2004)130:3(460).

Zeris, C. A. and Mahin, S. A. (1991) “Behaviour of reinforced concrete structures subjected to biaxial excitation,” J Struct Eng, 117(9), pp. 2657–2673.